SOLAR SPECTRAL IRRADIANCE VARIABILITY OF SOME CHROMOSPHERIC EMISSION LINES THROUGH THE SOLAR ACTIVITY CYCLES 21-23[*]

Ü. D. Göker[1,2], M. Sh. Gigolashvili[3] and N. Kapanadze[3]

[1]*Physics Department, Boğaziçi University, Bebek 34342, Istanbul, Turkey*

[2]*İstanbul Gelişim University, Faculty of Economics, Administrative and Social Sciences, Department of Aviation Management, Cihangir Quarter, Şehit Jandarma Komando Er Hakan Öner Street 1, Avcılar/İstanbul, Turkey*

E–mail: *udgoker@gelisim.edu.tr*

[3]*E. Kharadze Abastumani Astrophysical Observatory at Ilia State University, Kakutsa, Cholokashvili Ave 3/5, Tbilisi, 0162, Georgia*

E–mail: *natela.kapanadze@iliauni.edu.ge*

SUMMARY: A study of variations of solar spectral irradiance (SSI) in the wavelength ranges 121.5 nm-300.5 nm for the period 1981-2009 is presented. We used various data for ultraviolet (UV) spectral lines and international sunspot number (ISSN) from interactive data centers such as SME (NSSDC), UARS (GDAAC), SORCE (LISIRD) and SIDC, respectively. We reduced these data by using the MATLAB software package. In this respect, we revealed negative correlations of intensities of UV (289.5 nm-300.5 nm) spectral lines originating in the solar chromosphere with the ISSN index during the unusually prolonged minimum between the solar activity cycles (SACs) 23 and 24. We also compared our results with the variations of solar activity indices obtained by the ground-based telescopes. Therefore, we found that plage regions decrease while facular areas are increasing in SAC 23. However, the decrease in plage regions is seen in small sunspot groups (SGs), contrary to this, these regions in large SGs are comparable to previous SACs or even larger as is also seen in facular areas. Nevertheless, negative correlations between ISSN and SSI data indicate that these variations are in close connection with the classes of sunspots/SGs, faculae and plage regions. Finally, we applied the time series analysis of spectral lines corresponding to the wavelengths 121.5 nm-300.5 nm and made comparisons with the ISSN data. We found an unexpected increase in the 298.5 nm line for the Fe II ion. The variability of Fe II ion 298.5 nm line is in close connection with the facular areas and plage regions, and the sizes of these solar surface indices play an important role for the SSI variability, as well. So, we compared the connection between the sizes of faculae and plage regions, sunspots/SGs, chemical elements and SSI variability. Our future work will be the theoretical study of this connection and developing of a corresponding model.

Key words. Methods: data analysis – Sun: chromosphere – Sun: UV radiation

---

[*]This paper is dedicated to the memory of Prof. Marina Sh. Gigolashvili.

1. INTRODUCTION

The variability of solar spectral irradiance (SSI) in ultraviolet (UV) spectral range was significantly stronger in the last solar activity cycle (SAC) 23 than in the previous SACs 21 and 22. However, the cycle 23 did not behave as predicted: it was a magnetically weaker cycle and complex in terms of magnetic morphology (Gibson et al. 2011), it was weak in sunspot number and facular activity (de Toma et al. 2004), Mg II index and 10.7 cm solar radio flux (F10.7) than the two previous cycles 21 and 22 (Fisk and Zhao 2009). On the other hand, as has been argued in Krivova et al. (2003), the SSI variations in cycle 23 could not be explained in terms of surface magnetic features alone. It implies another or additional mechanisms such as sunspots, faculae, plages and chromospheric network for irradiance change.

We investigate an unexpected increase in SSI intensity for some spectral lines in the SAC 23 from our data analysis and correlate this increase with faculae and plage regions, and sunspot/sunspot group numbers and classes. In previous studies, the anomaly in SAC 23 was correlated with the international sunspot number (ISSN) observations alone rather than taking into account different sunspots and sunspot group classes and their structures, separately. The very specific and important studies of Lefévre and Clette (2011), Kilcik et al. (2011) and Kilcik et al. (2014) showed us the importance of the number and the class of small and large sunspots and/or sunspot groups (SGs) on the solar disc and their effects on the SACs.

In addition to this, helio-seismic data have also showed a surprising anti-correlation between frequencies and activity proxies during the minimum between SACs 23 and 24 (Tripathy et al. 2010). The heavy element abundances affect the helio-seismology by causing changes in the convection zone structure, and changes in the convection zone will affect the radiative opacities, the boundary between the radiative and convective zones and the equation of state (Basu and Antia 2004). The carbon group elements (e.g. carbon, silicon, germanium, tin and lead) and the bound-bound absorption of the metallic lines below 400 nm are the most important opacity sources (Fontenla et al. 1999).

From all these different points of view, the aim of this paper is the comparison of some selected SSI intensities for SACs 21-23 in the UV spectral range with the possible variations of chemical element ions corresponding to these wavelength ranges. We mainly concentrate our attention on this vari-

ation, in addition to this, we apply the variations of sunspots/SGs, plage regions, faculae and Ca II K-flux on the anomalies of the SSI variability between the spectral ranges 121.5 nm-300.5 nm and the changes in related chromospheric ions between the years 1981-2010.

The organization of the paper is as follows. In Section 2, we give the data description, clarify the data analysis technique and present the data analysis results for SSI, ISSN and spectral lines in the first part; we compare our results with sunspots/SGs, plage regions, faculae and Ca II K-flux which were taken by the ground-based telescopes in the second part. In Section 3, discussions about the data analysis results are presented and in Section 4, conclusions are given.

2. DATA DESCRIPTION, DATA ANALYSIS AND RESULTS

2.1. Data description and data analysis technique

The peculiarities of SAC 23 in the UV spectral range caused us to investigate the SSI variations for wavelengths 121.5 nm-300.5 nm to reveal possible special features of irradiance variations through SAC 23. Based on consideration of the abnormality of SAC 23, we decided to find out how well the irradiance variability of different spectral bands coincides with the ISSN for different SACs 21-23 and we estimated the existing correlations quantitatively.

Firstly, we investigated the SSI intensities in the range of 121.5 nm-300.5 nm for SACs 21, 22 and 23 obtained by Solar Mesosphere Explorer (SME)[†] for the years 1981-1990 (the available wavelength range 115.5 nm-302.5 nm), Upper Atmosphere Research Satellite[‡] (UARS) for the years 1992-2001 (the available wavelength range 119.5 nm-425.5 nm) and The Solar Radiation and Climate Experiment[§] (SORCE) for the years 2003-2009 (the available wavelength range 116.5 nm-1598.95 nm) experiments. Time series of SSI have been extracted from data centers of National Space Science Data Center[¶] (NSSDC), Goddard Distributed Active Archive Center[‖] (GDAAC) and LASP Interactive Solar Irradiance Data Center[**] (LISIRD) that served the archives of NASA space science mission data. The data contain hourly and daily measurements, and they are merged into ASCII text-files making data convenient. These different interactive data centers have taken the observational data for each 0.5 nm in the UV spectral range, so we made

---

[†]http://www.jpl.nasa.gov/missions/solar-mesosphere-explorer-sme/

[‡]http://uars.gsfc.nasa.gov/

[§]http://lasp.colorado.edu/home/sorce/

[¶]http://nssdc.gsfc.nasa.gov/

[‖]http://daac.gsfc.nasa.gov/

[**]http://lasp.colorado.edu/lisird/

our analysis for each 0.5 nm wavelength interval. A list of the selected data for UV spectral range used in the present analysis is given in Table 1. In this table, space flight experiments and data archives are indicated as well. The data processing includes:
(a) extracting and compiling of selected quantities;
(b) creation of the homogeneous local data set of formatted data;
(c) statistical processing of investigated data (regression analysis, correlation analysis).

The determination of SSI variability and finding accurate results below 400 nm is not easy. Investigations of de Toma et al. (2001) illustrate the difficulty in using simple proxies and regression techniques to deduce physical sources of SSI variability. Dudok de Wit et al. (2009) indicate that the best results for SSI have been taken from experimental data by using statistical analysis or by computing some special events. Besides analyzing techniques, there is another important problem with the choice of minimum days because the day-to-day solar irradiance variability is small at low levels of solar activity (Floyd et al. 1998). From this respect, we had to eliminate or reduce to a minimum the numbers of errors for these important problems to analyze the SSI variability.

Table 1. List of the selected data for UV spectral ranges used in the present analysis is given. The space flight experiments and data archives are indicated as well.

Selected Data for Processing and Origin Region	The Spaceflight Experiments and Data Archives				
	1981-1986 cycle 21-D[a]	1987-1990 cycle 22-A[b]	1992-1996 cycle 22-D	1997-2001 cycle 23-A	2003-2009 cycle 23-D
121.5 nm (Lyman α) emission Trans. Region	SME (NSSDC)	SME (NSSDC)	UARS (GDAAC)	UARS (GDAAC)	SORCE (LISIRD)
200.5 nm - 300.5 nm emission Chromosphere	SME (NSSDC)	SME (NSSDC)	UARS (GDAAC)	UARS (GDAAC)	SORCE (LISIRD)
ISSN Solar Surface	SIDC	SIDC	SIDC	SIDC	SIDC

[a] Descending
[b] Ascending

Table 2. Correlation coefficient values (with standard errors) correspond to the intensity profiles of the selected spectral lines with ISSN.

Spectral Lines	Correlation Coefficients (r_c)				
	1981-1986	1987-1990	1992-1996	1997-2001	2003-2009
121.5 nm	0.93±0.01	0.94±0.01	0.93±0.01	0.89±0.01	0.83±0.01
285.5 nm	0.76±0.02	0.31±0.03	0.37±0.03	0.54±0.02	0.03±0.02
300.5 nm	0.18±0.02	0.34±0.03	0.50±0.02	0.06±0.03	-0.74±0.01

Table 3. Correlation coefficient values (with standard errors) correspond to the standardized daily values of the selected spectral lines with ISSN.

Spectral Lines	Correlation Coefficients (r_c)				
	1981-1986	1987-1990	1992-1996	1997-2001	2003-2009
121.5 nm (Lyman α)	0.93±0.01	0.94±0.01	0.93±0.01	0.89±0.01	0.83±0.01
246.5 nm (Fe II)	0.87±0.01	0.90±0.01	0.86±0.01	0.85±0.01	0.77±0.01
279.5 nm (Mg II)	0.76±0.01	0.31±0.03	0.75±0.02	0.55±0.02	0.03±0.02
286.5 nm (Cr II)	0.66±0.02	0.28±0.03	-0.11±0.02	0.24±0.03	0.72±0.02
298.5 nm (Fe II)	0.42±0.02	0.03±0.03	-0.20±0.02	0.15±0.03	-0.73±0.02

Table 4. The estimation of coefficients of linear fits (with their errors) for relationships between SSI and ISSN for the SACs 21-23. The unit of slope "B" is given by W/m^2/nm.

I.P.S.S.L.*		Coefficients of Linear Fits				
		1981-1986	1987-1990	1992-1996	1997-2001	2003-2009
121.5 nm	B	(-3.36±0.07)×10^{-5}	(2.60±0.06)×10^{-5}	(-5.56±0.14)×10^{-5}	(5.08±0.08)×10^{-5}	(-6.02±0.06)×10^{-5}
	A	(5.46±0.23)×10^{-3}	(4.97±0.26)×10^{-3}	(7.94±0.26)×10^{-3}	(7.45±0.45)×10^{-3}	(6.94±0.36)×10^{-3}
285.5 nm	B	(-5.13±0.03)×10^{-4}	(4.26±0.02)×10^{-5}	(9.62±0.01)×10^{-5}	(1.44±0.01)×10^{-5}	(-1.61±0.01)×10^{-4}
	A	(6.93±0.60)×10^{-4}	(0.15±0.13)×10^{-3}	(0.32±5.39)×10^{-4}	(0.12±0.04)×10^{-3}	(0.36±0.03)×10^{-4}
300.5 nm	B	(-1.27±0.02)×10^{-3}	(2.70±0.01)×10^{-4}	(8.55±0.05)×10^{-5}	(1.04±0.34)×10^{-5}	(2.38±0.04)×10^{-4}
	A	(8.55±3.75)×10^{-4}	(1.30±0.41)×10^{-4}	(3.09±0.39)×10^{-4}	(3.85±1.20)×10^{-4}	(1.17±0.09)×10^{-4}
S.D.V.S.S.L.**		Coefficients of Linear Fits				
		1981-1986	1987-1990	1992-1996	1997-2001	2003-2009
121.5 nm	B	(-3.36±0.07)×10^{-5}	(2.60±0.06)×10^{-5}	(-5.56±0.14)×10^{-5}	(5.08±0.08)×10^{-5}	(-6.02±0.06)×10^{-5}
	A	(5.46±0.23)×10^{-3}	(4.97±0.26)×10^{-3}	(7.94±0.26)×10^{-3}	(7.45±0.45)×10^{-3}	(6.94±0.36)×10^{-3}
246.5 nm	B	(-0.67±0.01)×10^{-5}	(0.53±0.01)×10^{-5}	(-0.79±0.01)×10^{-5}	(0.86±0.01)×10^{-5}	(-2.86±0.02)×10^{-5}
	A	(5.38±0.02)×10^{-3}	(2.59±0.14)×10^{-3}	(4.06±0.18)×10^{-3}	(6.62±0.48)×10^{-3}	(6.35±0.44)×10^{-3}
279.5 nm	B	(-0.68±0.01)×10^{-5}	(0.53±0.01)×10^{-5}	(-0.80±0.02)×10^{-5}	(0.83±0.01)×10^{-5}	(-2.86±0.02)×10^{-5}
	A	(5.37±0.02)×10^{-3}	(2.58±0.20)×10^{-3}	(4.05±0.18)×10^{-3}	(6.62±0.47)×10^{-3}	(6.34±0.44)×10^{-3}
286.5 nm	B	(-5.10±0.03)×10^{-4}	(9.09±0.02)×10^{-4}	(9.60±0.03)×10^{-4}	(4.35±0.01)×10^{-4}	(-1.60±0.01)×10^{-4}
	A	(3.25±0.28)×10^{-3}	(7.29±2.62)×10^{-4}	(8.33±5.37)×10^{-4}	(3.07±1.26)×10^{-4}	(5.35±0.03)×10^{-4}
298.5 nm	B	(-1.27±0.02)×10^{-3}	(2.70±0.01)×10^{-4}	(8.30±0.05)×10^{-5}	(1.03±0.04)×10^{-3}	(3.40±0.04)×10^{-4}
	A	(2.55±3.75)×10^{-3}	(1.30±0.41)×10^{-4}	(3.12±0.39)×10^{-4}	(6.35±1.18)×10^{-4}	(1.83±0.21)×10^{-4}

* Intensity Profiles of the Selected Spectral Lines (Table 2)
** Standardized Daily Values of the Selected Spectral Lines (Table 3)

We chose the following wavelengths from the SSI database: 121.5 nm, 285.5 nm and 300.5 nm to analyze and compare the SSI variations of the selected bands with the chromospheric ions, and ISSN for the wavelenghts 121.5 nm, 246.5 nm, 279.5 nm, 286.5 nm and 298.5 nm. The ISSN data were obtained from the Solar Influences Data Analysis Center[††] (SIDC) and World Data Center[‡‡] for the Sunspot Index, at the Royal Observatory of Belgium. The 121.5 nm Lyman-α emission originates in the transition region of the Sun while 246.5 nm, 279.5 nm, 285.5 nm, 286.5 nm, 298.5 nm and 300.5 nm emission components of the SSI spectral lines originate in the solar chromosphere. Selected ASCII data have been reduced using MATLAB computing language. The statistical processing of the selected data includes the following steps:

(a*) **Interpolation of missing data**: Linear data interpolation was used in the case when data were missing. We interpolated daily values of data indices to get continuous and spectrally resolved measurements of the irradiance and more obvious trends of time series for SACs 21, 22 and 23.

(b*) **Primary processing of selected data (timed average, smoothed average)**: Since there were several data for a given day, we used the average values. The SSI data after the interpolation and timed/smoothed averaged processing are given in Figs. 1-3. These data will be used for regression analysis and standardization.

(c*) **Regression analysis of selected data to reveal linear trends**: For the linear regression we first calculated the estimated A and B coefficients:

$$y = A + Bx \,, \tag{1}$$

to find the equation of the best fit line above and the relationship between selected SSI and ISSN data by:

$$A = \frac{\sum_{i=1}^{n} \left(x_i^2 \bar{y} - (x_i y_i) \bar{x} \right)}{\Delta} \,, \tag{2}$$

$$B = \frac{\sum_{i=1}^{n} \left(x_i y_i - x_i \bar{y} \right)}{\Delta} \,, \tag{3}$$

$$\sigma_A^2 = \frac{\sigma_y^2}{N} \left(\frac{\sum_{i=1}^{n} x_i^2}{\Delta} \right) \,, \tag{4}$$

$$\sigma_B^2 = \left(\frac{\sigma_y^2}{\Delta} \right) \,, \tag{5}$$

where the independent variable x_i corresponds to 10-day averaged values selected from the ISSN data and the dependent variable y_i corresponds to the SSI data, N is the total number of data, i indicates the number of measurements, σ_A is the deviation of selected data for coefficient A, σ_B is the deviation of selected data for coefficient B and σ_y is the standard deviation for the selected SSI data. Δ and σ_y are given by:

$$\Delta = \sum_{i=1}^{n} \left(x_i^2 - x_i \bar{x} \right) \,, \tag{6}$$

$$\sigma_y^2 = \frac{1}{N-2} \sum_{i=1}^{n} (y_i - A - B x_i)^2 . \qquad (7)$$

We calculated the standard deviation for each case and estimated the accuracy of the linear trend coefficients. In Eq. (7), we added (N-2) as a denominator because this value gives us the best estimation result for the standard deviation of the selected data. The linear trends for the relationships between ISSN and 121.5 nm-300.5 nm spectral line intensities are computed by the least-squares method.

(d*) Determination and estimation of correlation coefficients for the time series of the selected data: To explore the correlation between the SSI variations and ISSN during SACs, we investigated a relationship between these parameters using the 10-day averaged data and calculated correlation coefficients (r_c) between intensity variations of separate SSI and ISSN data. We used the following equation:

$$r_c = \frac{\sum_{i=1}^{n} (x_i - \bar{x})(y_i - \bar{y})}{\left(\sum_{i=1}^{n} (x_i - \bar{x})^2 \sum_{i=1}^{n} (y_i - \bar{y})^2 \right)^{1/2}} , \qquad (8)$$

where x_i and y_i correspond to two different time series of running averaged values selected from the ISSN and SSI data, i indicates the number of measurements, and $\bar{x}$ and $\bar{y}$ are the time averaged values of the selected data. The r_c values for data smoothed by timed averages of 10 points for the years 1981-2001 and by moving averages of 61 points for the years 2003-2009 are found. We used different time/moving averages as "10" and "61" because we divided the sum of the daily data for the past 10 days by the number of days (10) to arrive at the 10-day average, however, a 61-day low-to-low cycle that turns back up is a high-probability pattern-recognition scheme. Especially, in the last SAC, applying moving averages of 61 points caused us to find high-probability calculation results to show the important changes in the decreasing phase of SAC 23. The r_c values corresponding to intensity profiles of the selected spectral lines are given in Table 2, and coefficients of determination (R^2) are stated in Figs. 1-3, as well. The detailed explanation of this method and its applications can be found in the work of Gigolashvili and Kapanadze (2012b).
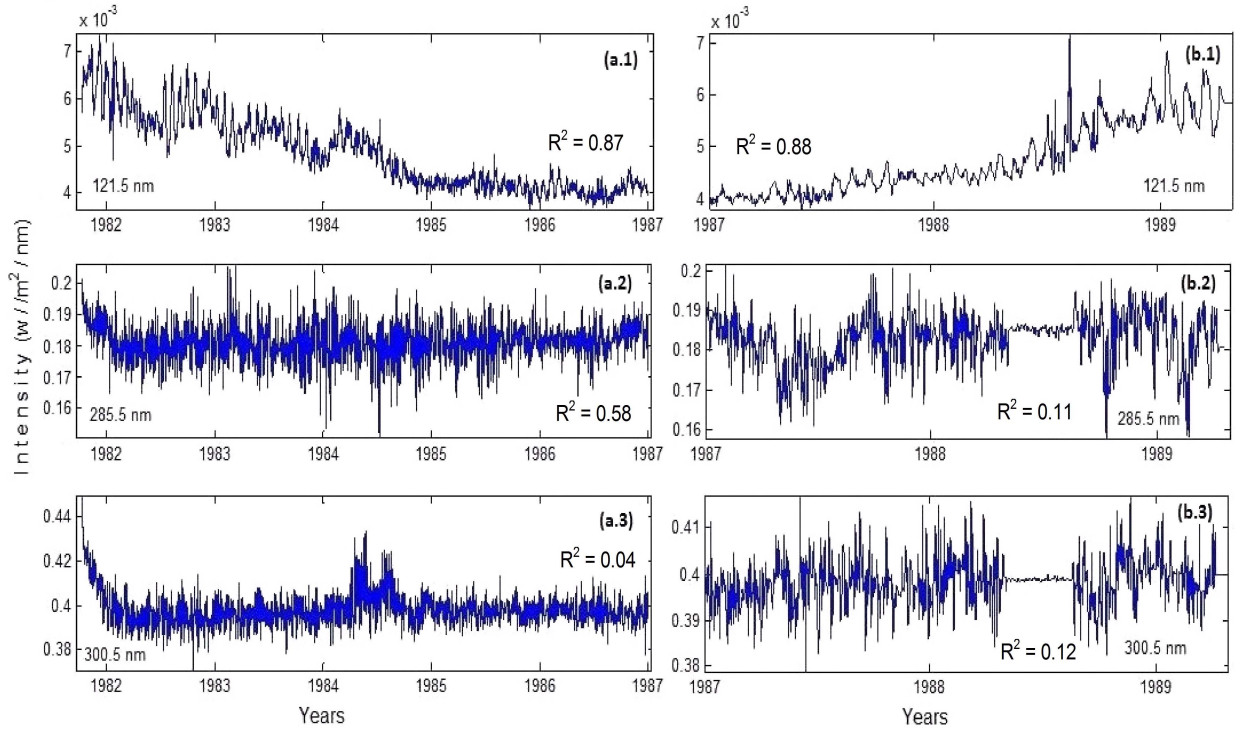
Fig. 1. *(a.1), (a.2), (a.3) indicate the SSI intensity data for 121.5 nm, 285.5 nm, 300.5 nm versus years for the descending phase of SAC 21 from 8 October 1981 to 31 December 1986, and (b.1), (b.2), (b.3) indicate the SSI intensity data for 121.5 nm, 285.5 nm, 300.5 nm versus years for the ascending phase of SAC 22 from 1 January 1987 to 13 May 1989. A relatively compatible correlation to SAC variation is observed for the SSI intensity of the selected spectral lines 121.5 nm, 285.5 nm and 300.5 nm from the year 1981 to 1990. However, coefficients of determination (R^2) values have still lower proportion of the variance for some wavelengths as seen in Figs. (b.2), (a.3) and (b.3).*
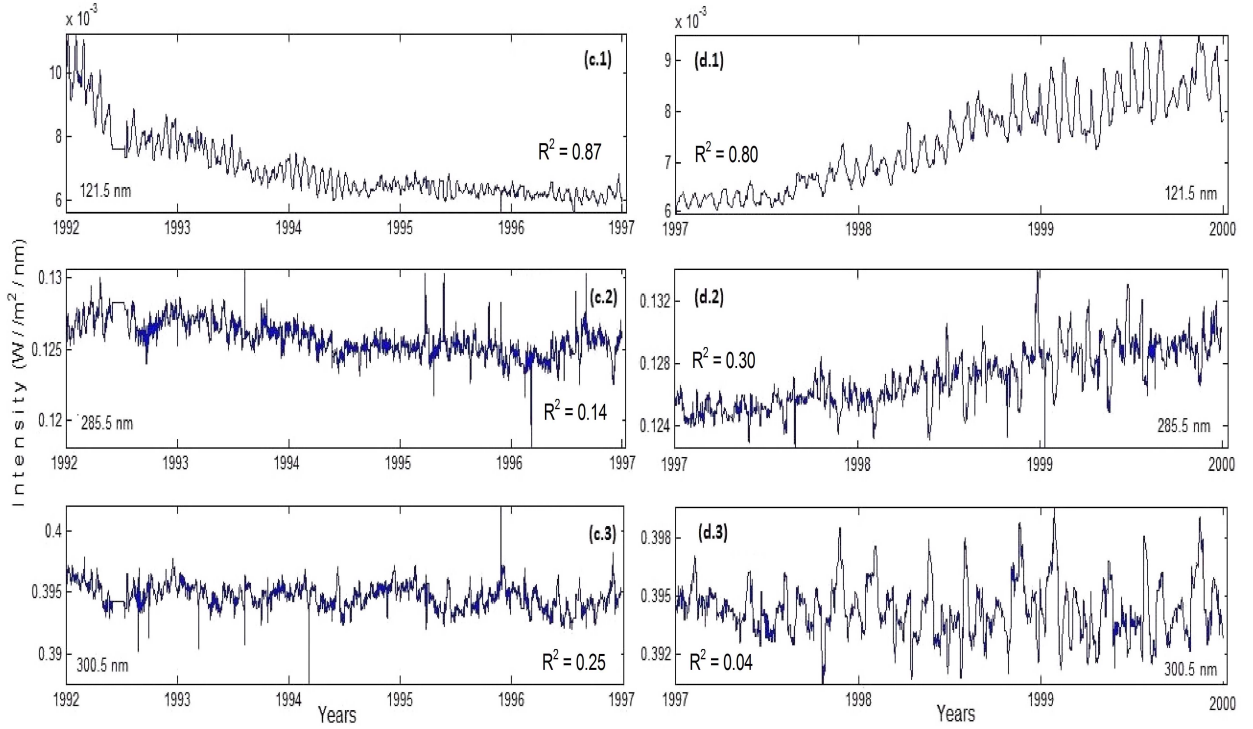
Fig. 2. (c.1), (c.2), (c.3) indicate the SSI intensity data for 121.5 nm, 285.5 nm, 300.5 nm versus years for the descending phase of SAC 22 from 31 December 1991 to 31 December 1996 and (d.1), (d.2), (d.3) indicate the SSI intensity data for 121.5 nm, 285.5 nm, 300.5 nm versus years for the ascending phase of SAC 23 from 1 January 1997 to 15 October 1999. A relatively compatible correlation to SAC variation is observed for the SSI intensity of the selected spectral lines 121.5 nm, 285.5 nm and 300.5 nm from the year 1991 to 2000. However, coefficients of determination (R^2) values have still lower proportion of the variance for some wavelengths as seen in Figs. (c.2), (c.3), (d.2) and (d.3).

2.2. Data analysis results

We examined more than twenty-five years of the SSI data obtained by space experiments in the previous section, and followed four processing steps to analyze the selected data. Secondly, the SSI and ISSN data were standardized by the equation:

$$y_s = \frac{y_i - \bar{y}}{\sigma_y}, \qquad (9)$$

where y_s is the standardized value, y_i is the daily value of time series of the selected data, $\bar{y}$ is the time averaged value of time series of the selected data, and σ_y is the standard deviation of time series of the selected data.

The magnetic field, sunspot number, facular activity, Mg II index, and F10.7 were lower depending on the 13 years length of SAC 23 but these lower values did not stop the increase of the SSI intensity in the 300.5 nm spectral line as seen in Fig.3. Therefore, this increasing caused us to investigate phenomena different from the previous studies, and we tried to connect this increase of the SSI intensity with the classes and the numbers of sunspots/sunspot groups, faculae and plage regions, and Ca II K index and

thereby investigate the possible elements corresponding to these wavelength ranges and examine whether these elements affect the increase or not. All the spectral lines between the ranges 121.5 nm - 300.5 nm and 200.5 nm - 300.5 nm were taken from the Harrison atlas (Harrison 1939) and the work of (Doschek et al. 1977), respectively.

Most of the chromospheric emission lines formed at temperatures below 2×10^4 K are emitted by chromospheric ions (Doschek et al. 1977). The main chromospheric emission lines for the 0.5 nm wavelength interval in the range 200.5 nm - 300.5 nm are C II, Co II, Cr II, Fe II, Mg II h&k line, Mn II, Ni II and Ti II, and all these emission lines are a function of wavelength (Haberreiter 2010).

The core of the Mg II line appeared in the chromosphere whereas the wings are generated in the upper photosphere which are insensitive to solar UV variations (Lilensten et al. 2008). The Mg II emission line intensity reduced by a few percent in the last SAC. The other important element Mn has less abundant Mn II ions which are optically thick close to the limb and it causes the decreasing of intensity (Doschek et al. 1977) while the widths of Si II (not in our wavelength range), C II, and metallic lines increase with height above the limb. In the chromo-
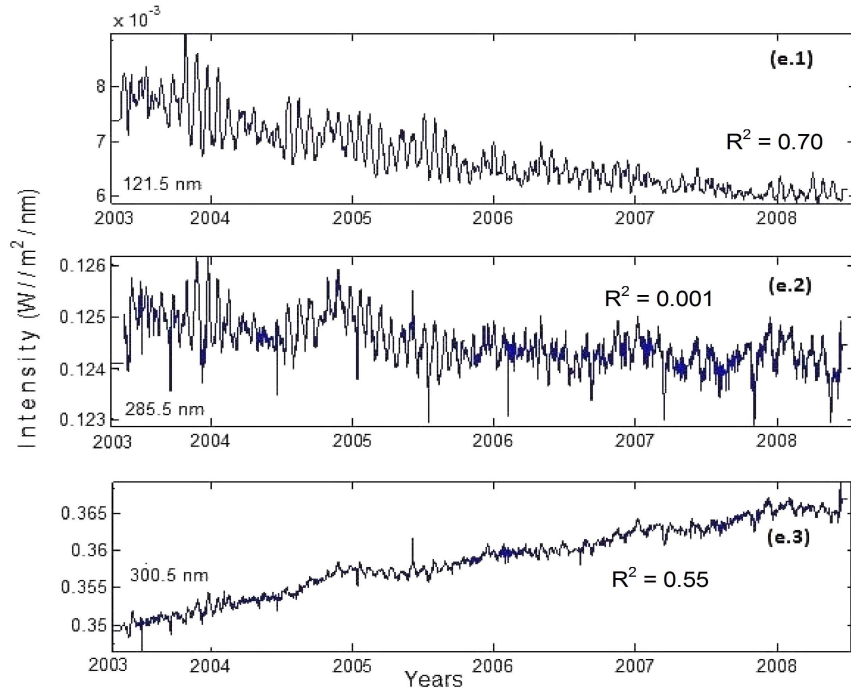
Fig. 3. *(e.1), (e.2), (e.3) indicate the SSI intensity data for 121.5 nm, 285.5 nm, 300.5 nm versus years for the descending phase of SAC 23 from 14 May 2003 to 14 June 2008. Positive correlation is observed for the SSI intensity of the selected spectral lines 121.5 nm and 300.5 nm from the year 2003 to 2009. In contrast to this, the correlation is not qualified for 285.5 nm as seen in Fig. (e.2) and this nonadaptive variation is supported by a very low coefficient of determination value such as $R^2 = 0.001$. In any case, it shows that the unexpected increasing of the 300.5 nm spectral line from the year 2003 to 2009 is caused by solar structure, and is not due to an instrumental effect. The high correlation value $R^2 = 0.55$ indicates this.*

sphere, these emission lines contribute to the formation of absorption spectral line profiles in SSI spectra.

From our analysis results, we found that only the Fe II (298.5 nm) chromospheric ion is dominant in the range 285.5 nm - 300.5 nm. In other wavelengths, the other chromospheric ions such as C II, Co II, Cr II, Mg II, Mn II, Ni II and Ti II also effect the intensity but not so much as the Fe II ion because the highest ionization stage only occurs for the metal iron. Ionization stage is related with the velocity: it becomes higher as the velocity increases and the density decreases. Increasing velocity also causes the increase of the acceleration and intensity. The standardized values of the emission components of the SSI spectral line intensities corresponding to these elements versus years are given in Figs. 4 and 5. The r_c values correspond to the standardized daily values of the selected spectral lines with ISSN which are shown in Figs. 4 and 5, are indicated in Table 3. Standardizing variables is very important for multivariate analysis. If we do not apply it, variables measured at different scales do not contribute equally to the analysis. Transforming the data to comparable scales prevents the huge difference between different scale variables as a variable with wide ranges will outweigh a variable with narrow ranges in boundary detection. So, standardization procedures equalize the range and/or data variability. In addition to this, we also stated the R^2 in Figs. 4 and 5.

The main idea here is that indicating the dominant chemical element ions correspond to upper and lower limits of selected spectral lines by showing SSI variations in specific wavelengths. In Figs. 1-3, the most important wavelengths (important for finding possible elements close to these -upper and lower limits- wavelengths) are given. In Figs. 4-5, we planned to analyze only chemical element ions and chromospheric emission components of SSI spectral lines corresponding to these wavelengths.

The most distinctive increase was seen for the Fe II (298.5 nm) spectral line in the UV spectral range through the descending phase of SAC 23 as seen in Fig. 5(a)-e and for the last years (since the middle of 1995) of the descending phase of SAC 22 (Fig. 4(c)-e) but we had to understand whether this increase is caused by the measurement error of changes of optical characteristics of measuring instruments or not. Therefore, we investigated intensity changes of two important emission lines for the plage regions, the Ca II K line (393.3 nm) and He I (587.59 nm), and they are shown in Figs. 5(b) and 5(c).

The Ca II K (393.3 nm) ions occurred in the upper photosphere and chromosphere which originated from the plage areas (Weber et al. 1998) and they are sensitive to the magnetic field (Gigolashvili and Kapanadze 2012a). Magnetically active structu-

77
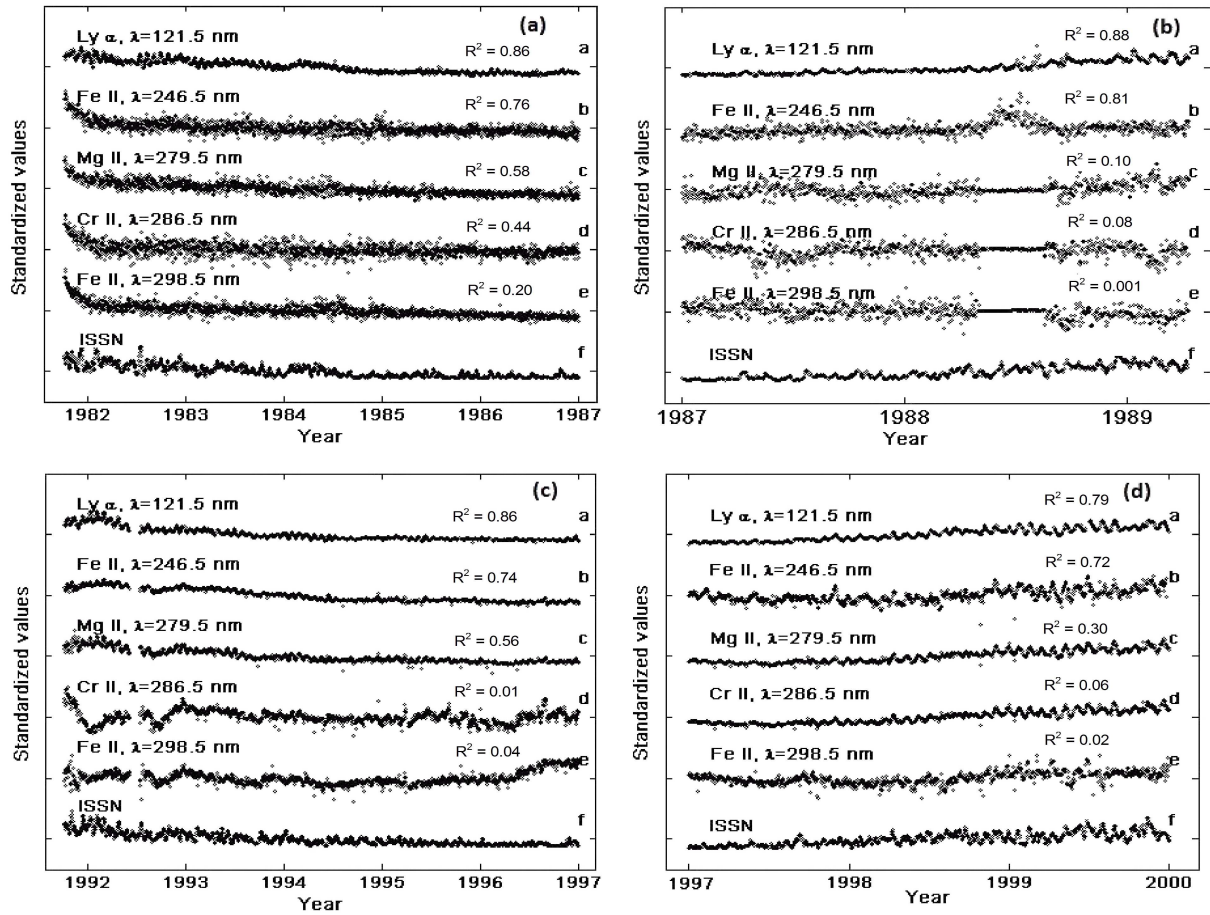
Fig. 4. *(a) From top to bottom (a-f), variations of standardized daily values of the selected band intensities with the corresponding elements 121.5 nm (Lyman α), 246.5 nm (Fe II), 279.5 nm (Mg II), 286.5 nm (Cr II), 298.5 nm (Fe II), and ISSN are given, respectively. Standardized values are shown as data points. Solid lines correspond to smoothed data created by moving average of 61 points. The horizontal axis corresponds to the period 8 October 1981 -31 December 1986. (b) The same parameters for the period 1 January 1987 - 13 May 1989. (c) The same parameters for the period 3 October 1991 - 31 December 1996. (d) The same parameters for the period 1 January 1997 - 15 October 1999. The only unexpected variation is seen for the Fe II element (298.5 nm) after the middle of 1996 for the decreasing phase of SAC22.*

res show a high contrast against the surrounding chromosphere. The Ca II K images give the possibility to see brightness along the edges of large convection cells called supergranules, and in areas called plages (Gigolashvili and Kapanadze 2012a).

Therefore, the Ca II K line provides important information on the large-scale magnetic field structure in the chromosphere. In addition to this, the He I 587.59 nm emission line also originates in the chromosphere and its emission line belongs to the visible range of the solar spectrum. This emission line is observed in prominences and plages, and it is also sensitive to magnetic fields.

The relation between the plage area (PA), the Ca II K line (393.3 nm) and He I (587.59 nm) line have been subject of many studies: the short-term variation of the central intensity of Ca II K_3 in 1979 which was clearly an integrated light signature of PA variability in 1981 has been indicated by Liv-

ingston and Holweger (1982); Fontenla et al. (1999) calculated the Ca II K and Mg II h&k indices for irradiance variations by taking into account the effects of sunspots, faculae, plage, network and quiet atmosphere but ignored the minor physical effects such as spicules, macrospicules and prominences to the SSI for SAC 22; absorption features of the He I D_3 line in plages have been studied in the work of Biazzo (2005); observation of the Ca II K images to estimate the contribution of the plages and the network to TSI at different epochs has been worked out by Parker (2010).

We used measurements extracted from the data center LISIRD and the same analyzing method for the spectral lines Ca II K and He I which we used for UV spectral lines. We found a decrease for Ca II K (393.36 nm) and an increase for He I (587.59 nm) for the years 2004-2009 (the decreasing phase of
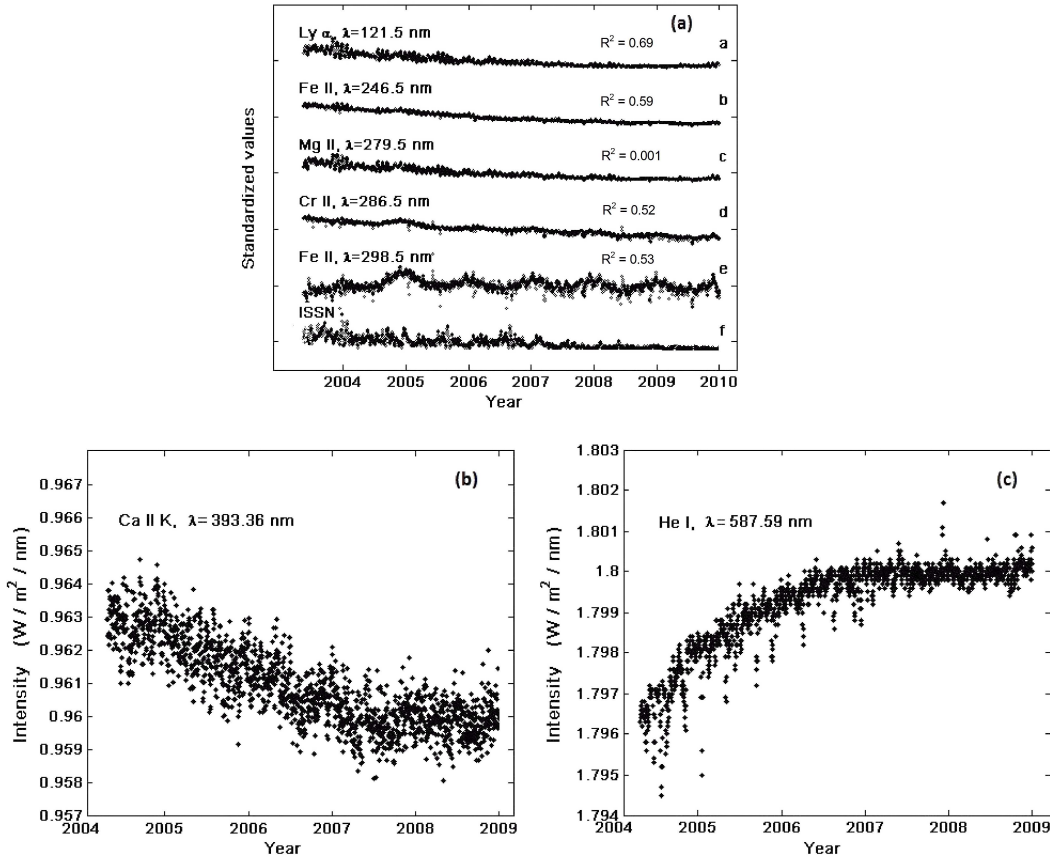
Fig. 5. *From top to bottom (a-f), variations of the standardized daily values of the selected band intensities with the corresponding elements 121.5 nm (Lyman α), 246.5 nm (Fe II), 279.5 nm (Mg II), 286.5 nm (Cr II), 298.5 nm (Fe II), and ISSN are given, respectively. Standardized values are shown as data points. Solid lines correspond to smoothed data created by moving average of 61 points. The horizontal axis corresponds to the period 14 May 2003 - 1 January 2010. Variations of the daily values of selected emission line Ca II K (393.36 nm) intensity (b), emission line He I (587.59 nm) intensity (c) are given as well. Data are shown with points. The horizontal axis corresponds to the period 1 March 2004 - 31 December 2008.*

SAC23) which are given in Figs. 5(b) and 5(c), and these results are compatible with the usual behavior of the Sun. This shows that our analysis method is applicable and instrumental errors were reduced to a minimum.

There are some gaps in observational data but these gaps originate from the satellites. The lower values of r_c and R^2 result from these gaps, not from the analyzing technique, because we have already reduced (and/or eliminated) the signal to noise ratio to a minimum. Therefore, we applied standardization techniques to these plots. However, we also dealt with the literature results which were related to possible errors in SORCE/SIM (Solar Irradiance Monitor) to see if these increases in the irradiance for the years 2003-2009 and spectral emission lines for the years 1995-1997 and 2003-2010 originate from instrumental errors.

The opposite trend at the end of SAC 23 for the irradiance observed by SORCE has already been reported in literature but this has been very much questioned since there is a disagreement with other data and models as in Ball et al. (2012), Ermolli et al. (2013), and Wehrli et al. (2013). SORCE satellite uses the UARS observations and these observations exhibit significantly larger variability in the UV, by almost a factor of 10 in the 200 nm-400 nm range. So, there might be an instrumental problem as over correction of the instrumental degradation at the origin of this opposite trend. In the paper of Ball et al. (2012), it was indicated that the 1630 nm-2423 nm and 300 nm-400 nm bands have a lower signal-to-noise ratio than the other bands. In the 200 nm-400 nm UV band, the trend is in phase with TSI while the trend is out of phase in the wavelengths 400 nm-1630 nm.

For wavelengths 120 nm-400 nm (corresponding to the Fe II (298.5 nm) and Ca II K line in our work) where the effective brightness temperature is less than $T_{eff} = 5770$ K, the irradiance decreases with decreasing solar activity while for the wavelength 587.5 nm (corresponding to He I in our

79

work) the effective brightness is greater than T_{eff} and the irradiance increases with decreasing solar activity. In our analysis, Figs. 5(b) and 5(c) correlate with the results in Ball et al. (2012) and the only increase was seen for the Fe II element (Figs. 4(c)-e and 5(a)). This result increases the possibility of the solar interior variability with the following years than instrumental errors.

On the other hand, Wehrli et al. (2013) mentioned that SORCE/SIM has published an unexpected negative correlation with TSI of the visible spectral range. In contrast to this, the same instrument shows a strong and positive variability of the near UV range. For the long-term uncertainties of the SIM instruments are $\approx$ 0.5-0.1%, $\approx$ 0.2-0.05%, and 0.05% for the wavelength ranges 200 nm-300 nm, 310 nm - 400 nm, and 400 nm - 1600 nm, respectively. Ermolli et al. (2013) mentioned that the instrument stability for long-term variations could be much lower than short-term variations. By comparisons of the VIRGO data observations of Wehrli et al. (2013) with the SORCE observations, based on the monthly snapshots, positive correlations of SSI with TSI were found for all three wavelengths while in the analysis of annual averages, the corrections at 862 nm and at 402 nm became negative and the negative correlation for the IR channel is more likely real than for the UV channel.

Computing regression coefficients and correlation coefficients, and comparing the standardized values are necessary to reach the more accurate results for the opposite trend between the SORCE irradiance at some wavelengths and the ISSN. Furthermore, in Figs. 5(b) and 5(c), we plotted the irradiance at wavelengths where chromospheric images are usually taken as the Ca II K line and He I. Our results are consistent with the results of Ball et al. (2012), however, new observations of SORCE should give the answer to the question of a possible error.

2.3. Data analysis results from the ground-based telescopes

In this section, we compared the time series analysis of the standardized values of SSI and ISSN with observations of sunspots/SGs, the Ca II K-flux, faculae, and plage regions taken by the ground-based telescopes. Sunspots which have different sizes and classes are one of the most important and prominent features on the solar surface (Kitiashvili 2012). Lefévre and Clette (2011) mentioned that SAC 23 was with particularly low and unique levels of the ISSN index and other solar indices. However, detailed statistics were obtained according to the group type and spot size in the works of Lefévre and Clette (2011), Kilcik et al. (2011) and Kilcik et al. (2014). It was found from these studies that the number of small spots show an important decrease from the year around 2000 while the number of large spots remained unaffected. In addition to this, there was also a global reduction of small SGs in SAC 23 compared to previous cycles. The ISSN is compatible with the sunspots/SGs while chromospheric ions are mostly related with faculae and plage regions.

Kilcik et al. (2011) found that the large sunspot group numbers (classes D, E, F and G) which contain penumbrae both in the main leading and following spots were lower during SAC 21 than those for SACs 22 and 23. They also mentioned that the total area of small (A and B (no penumbra), C, H and J (at least one main sunspot with penumbra)) sunspots/SGs in SAC 22 was larger than for SAC 23. In contrast to this, the averaged area of small sunspots was nearly the same in both SACs. In addition to this, the total area of large sunspots was larger while the total and the daily number of large SGs are nearly the same during SAC 22 as compared to SAC 23. The facular area (FA) arises to follow the large sunspot group numbers rather than the number of small SGs. The variations of the Ca II K line spectroheliograms at some observatories are of great importance because plages account for roughly one-half of the Sun's total magnetic flux, and most of the Sun's effect on the Earth originates from solar UV flux (Priyal et al. 2014).

It is considered that solar irradiance variations both the spectral and total are essentially caused by solar surface magnetism and thermal structures of magnetic features (sunspots, faculae) (Foukal 1992, Chapman et al. 1996, Fligge et al. 1998, Fligge et al. 2000, Krivova et al. 2003). Göker et al. (2016) examined a statistical analysis of solar activity indices "total solar irradiance (TSI), magnetic field, Ca II K-flux, faculae and plage areas due to the type of sunspots/SGs" through the SACs 21-23 and found interesting results that are connected with the chromospheric ions and SSI data. The main results from that paper are as follows:

(a) The number of AB and C type SGs is higher in the maximum of SACs 21 and 22 than in SAC 23, and it is the same in the minimum phase, as well. H groups have comparable numbers in the maximum phases of SACs 22 and 23, and no distinct data in the decreasing phase for some observing days as similarly seen in C type groups in SAC 23. However, in DEF groups there has been no important difference among all cycles.

(b) Both for small and large SGs start to appear before the magnetic field increasing occurs in SAC 23 while SGs and magnetic field are changing in a synchronized way in SAC 22. All small type SGs are lower in SAC 23 as compared to large SGs. Magnetic field is related with small SGs while TSI values are connected with large SGs (Göker et al. 2016, see Figs. 1 and 2).

(c) In SAC 23, large SGs reach their maximum numbers about 2 years later than the small ones and this time the difference is more effective for the magnetic field than in TSI. Small groups are efficient in TSI after the beginning of 1990 in SAC 22 and in the year 2000 of SAC 23 while large SGs show a double peak both in SACs 22 and 23 for the maximum phases of SACs, and they are dominant after the year 2002 in SAC 23 (Göker et al. 2016, see Fig. 2).

(d) Ca II K-flux is obviously lower in SAC 23 both for small and large SGs, however, the Ca II K-flux variations are comparable with C (essentially) and DEF type SGs while large SGs show higher correlation than the small SGs. Small SGs (especially AB type groups) correlate with the Ca II K-flux in SAC 22 while they move away from the correlation in SAC 23 (in the year 1999). FA and the Ca II K-flux are separated from synchronization in the beginning of 1999. FA starts to increase since the beginning of 1999 until the middle of 2009 and it starts to increase again after the year 2010. The small SGs (especially C groups) are comparable with the variation of the Ca II K-flux while we do not see such a correlation for FA (Göker et al. 2016, see Figs. 3 and 4).

(e) The coverage of FA on the solar surface is maximum during the year 1990 in SAC 22 while it is lower for SAC 23 in the year 2001. Similarly, the same decreasing is seen for the Ca II K-flux as well and it continues along with the decreasing phase of SAC 23. FA highly correlates with large SGs for both SACs rather than with small groups (Göker et al. 2016, see Figs. 3 and 4).

(f) The FA ratio decreases with increasing activity levels, whereas FA shows an increase in the decreasing phase of SAC 23. In the increasing phase of SAC 23, FA starts to increase from 1996 to 2000 because FA correlates with large SGs (Göker et al. 2016, see Figs. 3 and 4).

(g) The total (and the average) area of plages are decreased both for the descending and ascending phases of SAC 23. The PA correlates with C type of SGs more than with the other types. Especially, in the descending phases of SACs 22 and 23, DEF SGs reach their maximum values and C type SGs follow these DEF SGs in the second order. AB SGs are in the lowest values for the descending phase of SAC 23 and they are in the same number in the ascending phases of SACs 22 and 23. Only DEF SGs start their rising before PA started to appear, and the covered area of plages on the Sun decrease after the middle of the year 2002 (Göker et al. 2016, see Figs. 4 and 5).

(h) The FA evolve before the evolution of plage regions, and they reach maximum phases earlier than the PA. Large SGs are especially effective after the year 2002 and FA is even higher from the beginning of 2001 as opposite to the Ca II K-flux in SAC 23. The covered area of plages on the Sun decreases after the middle of the year 2002. FA has a strong influence on TSI while magnetic field is strongly related with plage regions. For the Ca II K-flux and plage regions, small SGs, especially C type SGs, are important.

3. DISCUSSIONS AND ANALYSIS RESULTS

The study of this paper is based on more than twenty-five years of SSI variations in the wavelength ranges 121.5 nm-300.5 nm for the period 1981-2009, and standardized values of emission components of SSI spectral lines and ISSN data analysis results for the period 1981-2010 from different interactive data centers. We reduced the selected data using the MATLAB computer programming.

From our data analysis results, we found a negative correlation of intensity of the UV (300.5 nm) spectral line (corresponds to the Fe II chemical element ion in 298.5 nm) originating in the solar chromosphere with the ISSN index during the minimum between SACs 23 and 24. Similar results for the UV spectral lines have been obtained by Amblard et al. (2008) using five years of daily EUV spectral data recorded by the TIMED/SEE (NASA Thermosphere Ionosphere Mesosphere Energetics and Dynamics/Solar EUV Experiment) satellite. Normally, the helio-seismic oscillations are associated with the inner part of the Sun while we are working on the solar chromosphere. However, Amblard et al. (2008) have found similar abnormal increases in their analysis and we thought that if something exists inside the Sun, it can easily affect the atmospheric layers.

Finally, we found the similar increases in the UV region in 300.5 nm and when we checked the chemical element ions, it corresponds to the value of the Fe II ion. The revealed negative correlations between sunspot numbers and some solar spectral bands of UV emission components and helio-seismic data (obtained by GONG and MDI) indicate that they are closely connected with the super-granules and plages (Dudok de Wit et al. 2009). Further, both the GONG and MDI frequencies show a surprising anti-correlation between frequencies and activity proxies during the minimum between SACs 23 and 24 (Tripathy et al. 2010). The main results that can be extracted from our study are as follows:

(1) In Figs. 1-3, the SSI intensity data for 121.5 nm, 285.5 nm, 300.5 nm versus years for the descending phase of SAC 21, ascending and descending phases of SACs 22 and 23 are given. As seen from Figs. 1 and 2, there is a positive variation according to activity processes for the SSI intensity of the selected spectral lines 121.5 nm, 285.5 nm and 300.5 nm. During the unusually prolonged minimum of SAC 23, an unexpected variation is investigated for the 300.5 nm spectral line from the years 2003 to 2009 as shown in Fig. 3-(e.3). The intensity variation interval for 300.5 nm is 4.2%, from 0.35 to 0.366 intensity value, for the descending phase of SAC 23. The high-frequency variabilities seen in the intensity profiles are caused by the sudden changes of daily data.

(2) As we know, the sense of the correlation may depend on the heights at which the flux-averaged contribution functions peak in various band-passes, and on how the sense of the correlation in any single band changes from one cycle to the next. In contrast to this, SAC 23 has got its own peculiarities and can be characterized as anomalous one. We calculated r_c and R^2 values for the Figs. 1-5. r_c measures a linear relationship between two variables (it changes between $-1 \leq r \leq 1$, here 1 indicates a perfect positive fit and -1 indicates a perfect negative fit) and R^2 represents the percentage of the data that is the closest to the line of best fit.

If the regression line passes exactly through every point on the scatter plot, it would be able to explain all of the variation. As it can be seen in Figs. 1-3, the best fit corresponds to 121.5 nm and only $10-20\%$ of the total variation remains unexplained in SACs 21-23. On the other hand, R^2 does not match 285.5 nm since the beginning of 1987 and the more unexplained value of R^2 emerges in SAC 23, however, the R^2 value gives relatively better results for 300.5 nm in the last SAC. This shows that the incompatible values of R^2 are not caused due to instrumental effects because all these chromospheric emission line data were taken from the same satellite observations. If one spectral line has a correlation problem, the other spectral lines should have it too but the results show the opposite of this relation. When we check the r_c values, there is a good correlation for 121.5 nm and 285.5 nm for the descending phase of SAC 21 while we do not see such correlation for other SACs. However, a good quality positive fit for 121.5 nm and ISSN variation appeared in the decreasing phase of SAC 23 and approximately a perfect negative fit is evident for 300.5 nm as well. Contrary to this, there is no correlation in 300.5 nm for SACs 21 and 22, and the ascending phase of SAC 23. It shows that the increasing number of large SGs caused the r_c values to give a relatively perfect fit and this result introduces the importance of the number and the class of sunspots/SGs in SACs. The ISSN and SSI profiles are compatible with sunspots/SGs while chromospheric emission lines (see Figs. 4 and 5) are mostly related with faculae and plage regions. Thus, this relation explains the negative fit of r_c in the descending phase of SAC 23 (especially for 300.5 nm) as seen in Fig. 3.

(3) When the stretch of SAC gets longer, the average temperature and the magnetic field intensity decrease. Decreasing temperature will cause the decrease of the radiation and intensity. As we know from literature, SAC 23 was also weak in sunspot number, facular activity, F10.7 and the area of bright faculae and chromospheric plages. Despite the fact that these parameters indicate lower values, the intensity increased in the descending phase of the last solar minimum. Therefore, we can say that the increase of the intensity is not affected directly by the temperature or the other well known parameters. Essentially, the affect of plage regions to the chromospheric radiation is already known and the plage regions are also very important for the SSI intensity because the most part of the SSI radiation is taken from the chromosphere. On the other hand, the determination of the SSI variability and finding accurate results below 400 nm is not easy, and the bound-bound absorption of the metallic lines below 400 nm are the most important opacity sources.

Thus, standardization of chromospheric emission lines below 400 nm is very important. Based on this, (a) the uncertainty of R^2 is maximum 30% for all cycles and a perfect positive fit with ISSN is clearly seen for 121.5 nm. The R^2 is a measure that allows us to determine how certain one can be in making predictions from a certain graph. From this, if $r_c = 0.84$, then $R^2 = 0.70$ which means that

70% of the total variation in y can be explained by the linear relationship between x and y. The other 30% of the total variation in y remains unexplained and it shows the uncertainty from the data. (b) The positive correlation of R^2 is in the higher values for SACs 21 and 22 and uncertainty is approximately 30% for 246.5 nm (Fe II) but through to SAC 23, the uncertainty of R^2 is increased while r_c is still in a good positive fit situation. (c) The more incompatible variation of R^2 with ISSN is clearly seen in the descending phase of SAC 23 for 279.5 nm (Mg II) and the best r_c value is seen in SACs 21 and 22. (d) The best R^2 value is examined in the decreasing phase of SAC 23 and depending on the negative value of r_c, we can say that Cr II (286.5 nm) is inversely proportional with the ISSN data in the decreasing phase of SAC 22. (e) The most distinct variation is seen in the decreasing phase of SAC 23 and this variation change is inversely proportional to the ISSN data. There is also an increase seen in the decreasing phase of SAC 22, especially from the year 1996, and it still continues to increase for 298.5 nm (Fe II) as seen in Figs. 4 and 5. The R^2 values are particularly higher in the decreasing phase of SACs because there are no extra disruptive effects of solar activities (e.g. flares, CMEs etc.) in this phase.

(4) In Table 4, we give the estimation of coefficients of linear fits (with their errors) for relationships between SSI and ISSN in Figs. 1-3 (intensity profiles of the selected spectral lines - I.P.S.S.L.) and Figs. 4-5 (standardized daily values of the selected spectral lines - S.D.V.S.S.L.) for SACs 21-23. In a linear regression analysis, the explanatory (x) and outcome (y) variables are linearly related while the linear regression coefficients A and B indicate the intercept and slope parameters in Eq. (1), respectively. The smaller error (or smaller p-value) value ($p \leq 0.05$) corresponds to a better fit while larger p-value suggests that changes in predictor are not associated with changes in the response. In other words, the p-value helps to determine the significance of results when a hypothesis test in statistical analysis is performed. The p-value is the probability that, using a given statistical model, the sample mean difference between two compared variables would be the same as or more extreme than the actual observed results when the null hypothesis is true. This hypothesis says that there is no statistical significance between the two variables if p-value is larger. In this situation, the null hypothesis can not be disproved and our statistical results move away from the best fit as opposed to the smaller p-value. The "best fit" for the data points means, as in the least-squares approach, a line that minimizes the sum of squared residuals of the linear regression model. If the p-value changes between $0.05 \leq p \leq 0.10$, it is defined as marginally significant. On the other hand, if the slope has a smaller relative error than the intercept, we can get more reliable estimates from the data. The slope parameter B shows the sign of the regression line. If B is negative, it corresponds to decrease of y values while x values are increasing as it can easily be

seen is Figs. (1)-(a.1)-(a.3), (2)-(c.1), (3)-(e.1)-(e.2), and Figs. 4(a), 4(c)-a, b, c and 5(a)-a, b, c, d. If B is positive, the line moves upward when going from left to right (x and y values change, simultaneously) as seen in Figs. (1)-(b.1)-(b.3), (2)-(c.2)-(c.3), (2)-(d.1)-(d.3), 3-(e.3), and Figs. 4(b), 4(c)-d, e, 4(d) and 5(a)-e.

Based on the explanations above, the best slope results with smaller errors can be seen for the I.P.S.S.L. and the S.D.V.S.S.L. as 285.5 nm and 300.5 nm, and 246.5 nm, 279.5 nm, 286.5 nm and 298.5 nm for the decreasing phases of SACs 21-23 and increasing phases of SACs 22-23 with approximately 95% confidence levels, respectively. Confidence bounds for the I.P.S.S.L. as 121.5 nm and 300.5 nm from the year 1981 to 2009 and 1992 to 2009 are approximately 86% and 85%, respectively while the S.D.V.S.S.L. as 121.5 nm, 246.5 nm, 279.5 nm from the year 1981 to 2003 are roughly 86%, 88% and 88%, and 298.5 nm from the year 1992 to 2009 is 80%. The estimation of coefficients of linear fits for the I.P.S.S.L. and the S.D.V.S.S.L. are consistent with each other, however, the best fit value is found for the descending phases of SACs 21-23. This shows that p-values are lower in the descending phase of activity cycles where extra distributive effects are lower. In spite of this, uncertainty occurs in higher values for the Fe II ion (298.5 nm) in the descending phases of SACs 22 and 23. Thus, it can be explained that higher p-values for the Fe II (298.5 nm) ion arise from different effects originates from Sun's itself. In addition to this, smaller relative errors of slopes for the I.P.S.S.L. and the S.D.V.S.S.L. than the intercept errors indicate more reliable estimations during SACs 21-23 as seen in Table 4.

(5) In the UV ranges of the spectrum, chromospheric metal ions are especially increased and this increase is more powerful for the metal iron for the descending phases of SACs 22 and 23 (298.5 nm) as seen in Figs. 4(c)-e and 5(a)-e. Ermolli et al. (2013) pointed out the stronger variability in the UV spectral range. So, any physical changes (e.g. the velocity, acceleration, the density, and the radius of the medium) that will occur in the UV region substantially effect the heavy element ions (especially iron in the present wavelength range). We also analyzed the two important chromospheric spectral lines such as the Ca II K line (393.36 nm) and He I (587.59 nm) which are related with the plage regions to prove our investigations for the Fe II chromospheric ion. From our analysis, we found decreasing and increasing intensities of the Ca II K line and He I which are given in Figs. 5(b) and 5(c), respectively. These results show us the accuracy of our data analysis because the radiation in the visible and infrared spectrum has a distinguishably different temporal character than the UV spectrum, particularly below 300 nm. Maximum energy changes occur at wavelengths from 400 to 500 nm while fractional changes are greatest at UV wavelengths (Singh et al. 2012). The intensity plots are different for the Ca II K and He I spectral lines because they appear on different solar areas as faculae, plage regions, and chromospheric network on the different solar layers such as the photosphere and chromosphere. Another reason for decreases and increases of the intensity of Ca II K and He I are their ionized and neutral characteristics, separately.

(6) ISSN and sunspot area are strongly correlated with each other, however, the effect of sunspot area is more important for the solar activity than the ISSN variability. Accordingly, small sunspot group numbers are generally connected with ISSN rather than large sunspot group numbers while FA shows better agreement with large sunspot group numbers. Nevertheless, the small and large sunspot group numbers show similar time variations only during SAC 22, AB and C type SGs are higher in SACs 21 and 22. The DEF groups have no important difference between all cycles and they are connected with TSI (and SSI) variations.

(7) In the declining phase, large SGs are important because the transportation of magnetic fields from the base of the convection zone to the solar surface is more efficient during the declining phase of SAC. Observations near the core of the ionized Ca II K line (393.37 nm) are one of the most effective tools to investigate the morphology and evolution of both plages and chromospheric magnetic network (Bertello, 2010). The total and average area of plages are decreased in SAC 23 and they correlate with C type SGs. The covered area of plages on the Sun decreased after the middle of the year 2002. FA starts to increase since 1996 until the middle of 2009 and it starts to increase again after the year 2010 because FA correlates with large SGs and large SGs are especially effective after the year 2002. FA evaluates before the evolution of plage regions and FA are higher from the beginning of 2001 opposite to the Ca II K-flux. Our time series analysis results on solar activity indices correlate with our statistical results on SSI, chemical element ions, and ISSN variations, because the SSI variation of 285.5 nm starts to deviate from the year 1992 to 2003 while 300.5 nm spectral line starts to increase after the year 1992 to 2010 (Figs. 2 and 3). The year 1996 is important because the increasing of FA in 1996 is caused by separation of FA and the Ca II K-flux from the synchronization in the beginning of 1999 and the coverage of FA on the solar surface is maximum in 1990. As we can see in Fig. 4(c)-e, the increase starts from the beginning of 1996 while it is lower in the declining phase of SAC 23 from the year 2003 to 2010 (Fig. 5(a)-e) and these increases of spectral line profiles correspond to the Fe II ion.

(8) This paper (and Göker et al. 2016) shows us the importance of the number and classes of sunspots/SGs, facular area, the Ca II K-flux, and plage region and their effect on SSI, chemical element ions and the ISSN variability. The small sunspots/SGs are important for intensity variations rather than the chromospheric ions while larger sunspot group numbers are effective for chromospheric (chemical element) ions.

4. CONCLUSIONS

An investigation of solar UV irradiance variability gives a good possibility for better understanding of physical processes existing on the Sun and global climate processes on Earth. Measurements of solar UV and FUV irradiance obtained by space experiments are particularly important because of their dominating role in solar-terrestrial connections.

The goal of our study is to investigate how well the irradiance variability of different UV wavelength bands coincides with the solar activity indices for different SACs and to estimate the existing correlation quantitatively. According to our study it is found that some chromospheric spectral lines do not agree equally well with the ISSN during the decreasing phases of SACs 22 and 23. Normally, the ascending phases of SACs are characterized by a relatively higher activity than the descending ones, but the descending phase of SAC 23 and the early stage of the ascending phase of SAC 24 have shown a particularly high-level of activity. The most distinctive increase is seen for the Fe II (298.5 nm) spectral line in the UV spectral range through the descending phase of SAC 23 and for the last years (since the middle of 1995) of the descending phase of SAC 22. Other increase is seen for the Cr II (286.5 nm) spectral line only in the descending phase of SAC 22. The anomalous activity from the beginning of SAC 23 can play a significant role in further development of SAC 24 and in forecasting of parameters for the upcoming cycle.

In the present paper, we give the analysis results of SSI and ISSN data, and suggest the connection of these parameters with chromospheric element ions from the corresponding spectral lines. We also connected these variations with faculae and plage regions, and the numbers and classes of sunspots/SGs. We found that ISSN is compatible with sunspots/SGs while chromospheric ions are mostly related with faculae and plage regions. The number of AB and C type SGs is higher in the maximum and minimum of SACs 21 and 22 than in SAC 23. However, in DEF groups there has been no important difference between all cycles. In SAC 23, large SGs reach their maximum number about 2 years later than the small ones and this time difference is more effective for magnetic field than in TSI. Small SGs (especially AB type groups) correlate with the Ca II K-flux in SAC 22 while they move away from the correlation in SAC 23 (in the year 1999) and FA arises to follow the large sunspot group (DEF type groups) numbers. FA and the Ca II K-flux are separated from the synchronization in the beginning of 1999 and FA starts to increase. PA correlates with C type SGs and the total (and the average) area of plages are decreased both for the descending and ascending phases of SAC 23. FA have strong influence on TSI while magnetic field is strongly related with plage regions. This relation explains the decrease of magnetic field and relatively unaffected variation of TSI in the last SAC 23. The effect of plage regions to chromospheric radiation is already known and the plage regions are also very important for the SSI in-tensity because the major part of the SSI radiation is taken from the chromosphere.

Our time series analysis results on solar activity indices correlate with our analysis results on SSI, chemical element ions, and ISSN variations. The distinct increase starts from the beginning of 1996 for the Fe II ion (298.5 nm) while it is lower in the decreasing phase of SAC 23 from the year 2003 to 2010 and this increase of the Fe II ion spectral line profile corresponds to the separation of FA and the Ca II K-flux from the synchronization in the beginning of 1999 and increasing of FA on the Sun. However, we need time series analysis of these spectral lines to relate with the solar activity indices for the following cycle 24 to find the exact correlation between these parameters. This is a different and long-term study, and SAC 24 will be a very good laboratory to analyze this feature in our next paper. Our findings may also influence our understanding of long-term variations of the SSI and TSI which is thought to be an important factor in the Sun-Earth climate relationship. Our results thus reveal the potential of such detailed SSI, FA and PA connection analyzes for understanding and predicting future trends of the chromospheric ions in SAC. Our future work will be the theoretical study of this connection and to develop a corresponding model.

REFERENCES

Amblard, P.-O., Moussaoui, S., Dudok de Wit, T., Aboudarham, J., Kretzschmar, M., Lilensten, J. and Auchère, F.: 2008, *Astron. Astrophys.*, **487**, L13.

Ball, W. T., Unruh, Y. C., Krivova, N. A., Solanki, S., Wenzler, T., Mortlock, D. J. and Jaffe, A. H.: 2012, *Astron. Astrophys.*, **541**, 27.

Basu, S. and Antia, H. M.: 2004, *Astrophys. J.*, **606**, L85.

Bertello, L., Ulrich, R. K. and Boyden, J. E.: 2010, *Solar Phys.*, **264**, 31.

Biazzo, K.: 2005, PhD Thesis, Università Degli Studi di Catania.

Chapman, G. A., Cookson, A. M. and Dobias, J. J.: 1996, *J. Geophys. Res.*, **101**, 13541.

de Toma, G., White, O. R., Chapman, G. A., Walton, S. R., Preminger, D. G., Cookson, A. M. and Harvey, K. L.: 2001, *Astrophys. J.*, **549**, L131.

de Toma, G., White, O. R., Chapman, G. A., Walton, S. R., Preminger, D. G. and Cookson, A. M.: 2004, *Astrophys. J.*, **609**, 1140.

Doschek, G. A., Cohen, L. and Feldman, U.: 1977, *Astrophys. J. Suppl. Ser.*, **33**, 101.

Dudok de Wit, T. D., Kretzschmar, M., Lilensten, J. and Woods, T.: 2009, *Geophys. Res.*, **36**, L10107.

Ermolli, I., Matthes, K., Dudok de Wit, T., Krivova, N. A., Tourpali, K., Weber, M., Unruh, Y. C., Gray, L., Langematz, U., Pilewskie, P., Rozanov, E., Schmutz, W., Shapiro, A., Solanki, S. K. and Woods, T. N.: 2013, *Atmosp. Chem. and Phys.*, **13**, 3945.

Fisk, L. A. and Zhao, L.: 2009, *IAU Symp.*, **257**, 109.

Fligge, M., Solanki, S. K., Unruh, Y. C., Fröhlich, C. and Wehrly, Ch.: 1998, *Astron. Astrophys.*, **335**, 709.

Fligge, M. Solanki, S. K. and Unruh, Y. C.: 2000, *Astron. Astrophys.*, **353**, 380.

Floyd, L. E., Reiser, P. A., Crane, P. C., Herring, L. C., Prinz, D. K. and Brueckner, G. E.: 1998, *Solar Phys.*, **177**, 79.

Fontenla, J., White, O. R., Fox, P. A., Avrett, E. H. and Kurucz, R. L.: 1999, *Astrophys. J.*, **518**, 480.

Foukal, P.: 1992, *ASP Conf. Series*, **27**, 439.

Gibson, S. E., de Toma, G., Emery, B., Riley, P., Zhao, L., Elsworth, Y., Leamon, R. J., Lei, J., McIntosh, S., Mewaldt, R. A., Thompson, B. J. and Webb, D.: 2011, *Solar Phys.*, **274**, 5.

Gigolashvili, M. Sh. and Kapanadze, N. G.: 2012a, in "Natural Cataclysms and Global Problems of the Modern Civilization" Proc. of the World Forum International Congress, SWB, London, **621**, 367.

Gigolashvili, M. Sh. and Kapanadze, N. G.: 2012b, *Sun and Geosp.*, **7**, 35.

Göker, Ü. D., Singh, J., Nutku, F. and Priyal, M: 2016, arXiv:1604.03011v1.

Haberreiter, M.: 2010, *IAU Symp.*, **264**, 231.

Harrison, G. R.: 1939, Wavelength Tables, The Technology Press-MIT, Cambridge MA; J. Wiley and Sons Inc., New York; Chapman and Hall Ltd., London.

Kilcik, A., Özgüç, A., Yurchyshyn, V. B. and Rozelot, J. P.: 2011, *Astrophys. J.*, **731**, 30.

Kilcik, A., Yurchyshyn, V. B., Abramenko, V., Goode, P. R., Özgüç, A., Rozelt, J. P. and Cao, W.: 2014, *Solar Phys.*, **289**, 4365.

Kitiashvili, I.: 2012, *IAU Symp.*, **294**, 269.

Krivova, N. A., Solanki, S. K., Fligge, M. and Unruh, Y. C.: 2003, *Astron. Astrophys.*, **399**, L1.

Lefévre, L. and Clette, F.: 2011, *Astron. Astrophys.*, **536**, L11.

Lilensten, J., Dudok de Wit, T., Kretzschmar, M., Amblard, P.-O., Moussaoui, S., Aboudarham, J. and Auchère, F.: 2008, *Ann. Geophys.*, **26**, 269.

Livingston, W. and Holweger, H.: 1982, *Astrophys. J.*, **252**, 375.

Parker, D. G.: 2010, PhD Thesis, University of California.

Priyal, M., Singh, J., Ravindra, B., Priya, T. G. and Amareswari, K.: 2014, *Solar Phys.*, **289**, 137.

Singh, J., Belur, R., Raju, S., Pichaimani, K., Priyal, M., Gopalan Priya, T. and Kotikalapudi, A.: 2012, *Res. Astron. Astrophys.*, **12**, 201.

Tripathy, S. C., Jain, K., Hill, F. and Leibacher, J. W.: 2010, *Astrophys. J.*, **711**, L84.

Weber, M., Burrows, J. P. and Cebula, R. P.: 1998, *Solar Phys.*, **177**, 63.

Wehrli, C., Schmutz, W. and Shapiro, A. I.: 2013, *Astron. Astrophys.*, **556**, 3.

ВАРИЈАЦИЈА СПЕКТРАЛНЕ ИНСОЛАЦИЈЕ У НЕКИМ ХРОМОСФЕРСКИМ ЕМИСИОНИМ ЛИНИЈАМА ТОКОМ ЦИКЛУСА СУНЧЕВЕ АКТИВНОСТИ 21-23

Ü. D. Göker[1,2], **M. Sh. Gigolashvili**[3] **and N. Kapanadze**[3]

[1]*Physics Department, Boğaziçi University, Bebek 34342, Istanbul, Turkey*

[2]*İstanbul Gelişim University, Faculty of Economics, Administrative and Social Sciences, Department of Aviation Management, Cihangir Quarter, Şehit Jandarma Komando Er Hakan Öner Street 1, Avcılar/İstanbul, Turkey*

E–mail: *udgoker@gelisim.edu.tr*

[3]*E. Kharadze Abastumani Astrophysical Observatory at Ilia State University, Kakutsa, Cholokashvili Ave 3/5, Tbilisi, 0162, Georgia*

E–mail: *natela.kapanadze@iliauni.edu.ge*

Представљамо проучавање варијације спектралне инсолације (SSI у опсегу таласних дужина од 121.5 nm – 300.5 nm, за период од 1981–2009. године. Користили смо различите податке за спектралне линије из ултраљубичасте области (UV) и међународни број Сунчевих пега (ISSN) из интерактивних база података као што су SME (NSSDC), UARS (GDAAC), SORCE (LISIRD) и SIDC, тим редом. Редуковали смо ове податке користећи програмски пакет MATLAB. На овај начин открили смо антикорелацију између интензитета UV (121.5 nm – 300.5 nm) спектралних линија које потичу из хромосфере и ISSN индекса током неуобичајено продуженог минимума између 23 и 24 циклуса Сунчеве активности (SAC). Такође, упоредили смо наше резултате са варијацијама индекса Сунчеве активности које су добијене са телескопа на земљи. Нашли смо да се области плажа смањују, а факуле се повећавају у SAC 23. Смањивање области плажа је уочено код малих група Сунчевих пега. Насупрот томе, ови региони код великих пега су упоредиви са претходним SAC или чак и већи, што је такође случај и са факулама. Без обзира на то, антикорелација између ISSN и SSI података указује да су ове варијације у блиској вези са класама Сучевих пега, факулама и плажама. На крају смо анализирали временске серије спектралних линија које одговарају таласним дужинама од 121.5 nm – 300.5 nm, и упоредили их са ISSN подацима. Нашли смо неочекивани пораст на 298.5 nm, који одговара линији јона Fe II. Варијабилност линије јона Fe II (298.5 nm) је у блиској вези са факулама и плажама, а величина ових индекса везаних за регионе Сунчеве површине игра битну улогу у варијабилности SSI. Наш будући рад биће теоријска студија ових веза и развој модела који их описује.